ance. The reflection coefficient was measured using a dual directional coupler and a swept amplitude analyzer. Matching of the periodic line was accomplished using a taper. A tapered line of suitable length was used at the input end of an eight-section periodic structure fabricated on a substrate with $\epsilon_r = 10.2$. A 50-Ω load was connected at the other end using a microstrip connector. Initial calibration was done with an identical input tapered line which was shorted at the end. Fig. 9 shows the measured input reflection coefficient of the eight-section periodic structure.

The same setup was used for the measurement of insertion loss. It ascertains, as shown in Fig. 7, the frequency characteristics of the bandstop filter. These characteristics are discussed in the following section.

V. Results and Discussion

In Fig. 3, the experimental points closely follow the theoretical curves. However, they deviate at the higher frequencies. This may be attributed to the presence of hybrid modes, and dielectric and radiation losses. Also, it can be observed that the stopbands grow wider as m increases. The phase and group velocities (Fig. 5) are found to be almost constant over a fairly large portion of the passband.

The return-loss measurement shows a moderate amount of ripple in the passband. This is expected from the expression for the input impedance. It may be noted from Fig. 4 that the characteristic impedance is not very sensitive to frequency in the passband, and hence broad-band matching may not be difficult to achieve. The theoretical (Fig. 8) and experimental (Fig. 9) curves of the input reflection coefficient show fairly good agreement. It is also seen in Fig. 8 that with loads lower than 50 Ω, the ripple in the passband is reduced in the frequency range below the stopband and vice versa at frequencies above the stopband. This is also evident in Fig. 4.

The frequency response of the bandstop filter (Fig. 7) shows that its insertion loss increases with m. A frequency shift away from the theoretically predicted value of $f_0 = 5.3$ GHz can also be observed in Fig. 7. For $m = 0.4$, the measured shift of center frequency is 0.4 GHz, whereas it is only 0.05 GHz for $m = 0.6$. At a 6-dB insertion loss, the bandwidths are found to be 1.6 GHz (for $m = 0.4$) and 2.4 GHz (for $m = 0.6$). While the first value agrees exactly with the design data, the second differs by $+0.05$ GHz from the theoretical value.

VI. Conclusion

An analysis of a sinusoidally modulated microstrip periodic line is given. An experimental investigation has been carried out on lines with several values of p and m. In all cases, the experimental results by and large agree with the theory as already discussed. The matching problem has to be improved. This can be achieved to some extent by using substrates of low ϵ_r with W_0 corresponding to 50 Ω. Also, the effect of fabrication tolerance is reduced in this case.

The bandstop filter is very easy to design. Its characteristics can be varied by changing p and m. The response has steep skirts. It may perform better than the conventional type of filters.

References

[1] C. P. Womack, "The use of exponential transmission lines in microwave components," *IRE Trans Microwave Theory Tech.*, vol. MTT-10, pp. 124–132, Mar. 1962.

[2] R. N. Ghose, *Microwave Circuit Theory and Analysis*. New York: McGraw-Hill, 1963, ch. 12.

[3] R. N. Ghose, "Exponential transmission lines as resonators and transformers," *IRE Trans. Microwave Theory Tech.*, vol. MTT-5, pp 213–217, July 1957.

[4] H. J Scott, "The hyperbolic transmission line as a matching section," *Proc. IRE*, vol. 41, pp. 1654–1657, Nov. 1953.

[5] E. N. Protonatorios and O. Wing, "Analysis and intrinsic properties of the general non-uniform transmission line," *IEEE Trans. Microwave Theory Tech* , vol. MTT-15, pp. 142–150, Mar 1967.

[6] S. Yamamoto, T. Azakami, and K Itakura, "Coupled non-uniform transmission lines and its applications," *IEEE Trans. Microwave Theory Tech* , vol MTT-15, pp 220–231, Apr. 1967.

[7] A. K. Sharma and B Bhat, "Analysis of coupled non-uniform transmission line two-port networks," *Arch. Elek. Ubertragung*, vol 32, pp. 334–337, 1978.

[8] S. C. Dutta Roy, "Matrix parameters of non-uniform transmission lines," *IEEE Trans. Circuit Theory*, vol. CT-12, pp. 142–143, Mar. 1965.

[9] M. I. Sobhy and E. A. Hosny, "The design of directional couplers using exponential lines in inhomogeneous media," *IEEE Trans. Microwave Theory Tech.*, vol. MTT-30, pp 71–76, Jan. 1982.

[10] R. E Collin, *Foundations for Microwave Engineering*. New York: McGraw-Hill, 1966, ch 8.

[11] A K. Mallick and G. S. Sanyal, "Electromagnetic wave propagation in a rectangular waveguide with sinusoidally varying width," *IEEE Trans. Microwave Theory Tech.*, vol. MTT-26, pp. 243–249, Apr. 1978.

[12] P. Benedek and P Silverster, "Equivalent capacitances for microstrip gaps and steps," *IEEE Trans. Microwave Theory Tech.*, vol. MTT-20, pp. 729–733, Nov 1972.

[13] C. Gupta and A. Gopinath, "Equivalent circuit capacitance of microstrip step change in width," *IEEE Trans. Microwave Theory Tech.*, vol. MTT-25, pp. 819–822, Oct. 1977.

[14] R Garg and I J Bahl, "Microstrip discontinuities," *Int J. Electron.*, vol 45, no 1, pp 81–87, July 1978

[15] H A. Wheeler, "Transmission line properties of strip on a dielectric sheet on a plane," *IEEE Trans. Microwave Theory Tech.*, vol. MTT-25, pp. 631–647, Aug. 1977.

[16] M. V. Schneider, "Microstrip lines for microwave integrated circuits", *Bell Syst. Tech J.*, vol 48, no 5, pp. 1421–1444, May 1969.

[17] J. C. Slater, *Microwave Electronics*. New York: Van Nostrand, 1950, ch. 8.

[18] M. D. Sirkis, "Application of perturbation theory to the calculation of $\omega-\beta$ characteristics for periodic structure," *IRE Trans. Microwave Theory Tech.*, pp 251–252, Mar. 1960.

[19] D A. Watkins, *Topics in Electromagnetic Theory*. New York: Wiley, 1958, p. 9.

Semiconductor Antenna: A New Device in Millimeter- and Submillimeter-Wave Integrated Circuits

F. C. JAIN, MEMBER, IEEE, R. BANSAL, MEMBER, IEEE, AND C. V VALERIO, JR., MEMBER, IEEE

Abstract **— A new approach in realizing millimeter- and submillimeter-wave antennas using semiconductor materials is described. The characteristics of these antennas can be controlled during fabrication and/or during operation by modulating the conductivity of the semiconductor. Theoretical computations are presented to evaluate the performance of some typical antenna structures. The physical layout of a monolithic semiconductor antenna with its associated control elements is also described.**

I. Introduction

Recent advances [1] in the monolithic integrated circuit technology for millimeter-wave systems have provided a new impetus to the design of compatible circuit components. This paper describes a new approach [2] in the realization of millimeter- and

Manuscript received June 15, 1983; revised September 14, 1983.

F. C. Jain and R Bansal are with the Department of Electrical Engineering and Computer Science, University of Connecticut, Storrs, CT 06268.

C. V. Valerio is with the Phonon Corporation, Simsbury, CT 06070.

0018-9480/84/0200-0204$01.00 ©1984 IEEE

submillimeter-wave antennas using doped semiconductor films grown on suitable semiconductor/insulator substrates. Such antenna configurations can be integrated readily with other semiconductor devices in various applications including high-resolution airborne radar [3].

The radiation characteristics of a dipole antenna are known to depend significantly on the current distribution along its length. Conventional millimeter- and submillimeter-wave antennas, such as microstrip dipoles and patches [4], are fabricated from high-conductivity metallic coatings. These structures have little or no control over the current distribution by the manipulation of material properties. In contrast, the radiation and circuit characteristics of the semiconductor antennas are closely related to the value of conductivity and its variation along the antenna length. It is shown, for example, that a pure traveling-wave-type current distribution with its concomitant broad-band and directional properties can be realized by the incorporation of a suitably tapered conductivity profile.

II. Theory

The performance of simple semiconductor antenna structures, such as solid whiskers and tubular dipoles, can be analyzed on the basis of earlier theoretical work of King *et al.* [5]–[7] on resistive antennas. These cylinderical geometries can be related to their planar counterparts in monolithic configurations through the "equivalent radii" concept [8], [9]. The effect of the insulating substrate on the radiation characteristics of the antenna is not taken into account in the present analysis to keep the mathematical formulation and numerical computations tractable. For printed metallic dipoles, the effect of the substrate has been recently studied by Rana and Alexopoulos [10]. A similar approach is currently under investigation for semiconductor antennas described in Section IV.

Fig. 1 shows two antenna configurations analyzed in this paper. Fig. 1(a) is a solid semiconductor whisker, while the antenna in Fig. 1(b) consists of a semiconductor coating over an insulating tubular substrate. Both structures are driven at their centers by delta-function generators with an EMF V_0^e. An integral equation can be formulated for the current along these antennas, and an approximate solution can be obtained in terms of simple trigonometric functions. Furthermore, a distribution of internal impedence per unit length can be determined that would yield a pure traveling current wave with no reflected component.

Since the theoretical development below closely parallels the analysis of King *et al.* [5]–[7], most of the details have been omitted here and only the essential results have been described. However, it should be emphasized that the approximations employed in [5]–[7] have been thoroughly checked for the parameters of the millimeter-wave semiconductor antennas.

The axial component $A_z(z)$ of the vector potential on the surface of the cylindrical antenna of Fig. 1(a) or 1(b) is related to the total axial current $I_z(z)$ through the following one-dimensional wave equation

$$\left(\frac{\partial^2}{\partial z^2}+k_0^2\right)A_z(z)=\frac{jk_0^2}{\omega}\left[Z'(z)I_z(z)-V_0^e\,\delta(z)\right] \tag{1}$$

where $Z'(z)=r'(z)+jx'(z)$ is the internal impedance per unit length and $k_0=\omega/c=2\pi/\lambda$ is the free-space wavenumber. The time dependence is assumed to be $e^{j\omega t}$. For the cases analyzed in this paper, the displacement current is essentially negligible as compared to the conduction current in the semiconductor antenna. Two specific distributions of $Z'(z)$ are considered next.

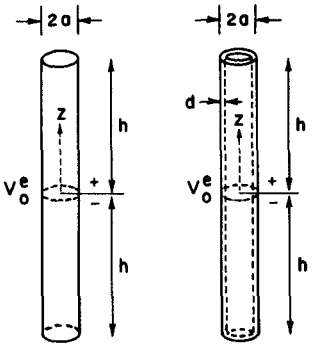

Fig. 1 Dipole antenna configurations: (a) solid semiconductor whisker, (b) tubular dipole with semiconductor coating.

Case I: Antenna with Constant Internal Impedance per Unit Length

When the internal impedance per unit length is constant, an approximate solution of (1) can be obtained in the following form [5]:

$$I_z(z)=\frac{j2\pi k_0 V_0^e}{\zeta_0 k\psi_{dR}\cos kh}\cdot\left[\sin k(h-|z|)+T_U(\cos kz-\cos kh)+T_D\left(\cos\frac{1}{2}k_0 z-\cos\frac{1}{2}k_0 h\right)\right] \tag{2}$$

where ψ_{dR}, T_U, and T_D are coefficients defined in King and Wu's work [5]; $\zeta_0=\sqrt{\mu_0/\epsilon_0}\simeq 377\ \Omega$, and the complex wavenumber k is defined by

$$k=\beta-j\alpha=k_0\left[1-\frac{j4\pi Z'}{k_0\zeta_0\psi_{dR}}\right]^{1/2}. \tag{3}$$

Once the current distribution $I_z(z)$ is known, other antenna characteristics can be derived in a straightforward manner. In particular, the input admittance Y and the radiation efficiency η are related to $I_z(z)$ through

$$Y=\frac{I_z(0)}{V_0^e} \tag{4}$$

and

$$\eta=\frac{\text{Power radiated}}{(\text{Power radiated}+\text{Power dissipated})}=1-\frac{r'\,\text{Re}(Y)}{|I(0)|^2}\int_{-h}^{h}|I(z)|^2\,dz. \tag{5}$$

Alternative expressions that are useful when k is predominantly real ($\alpha\ll\beta$) and βh is at or near $\pi/2$ are in the literature [5], [6].

Case II: Antenna with Variable Internal Impedance

When the internal impedance per unit length is given by

$$Z'(z)=\frac{\zeta_0\psi}{2\pi(h-|z|)} \tag{6}$$

where

$$\psi=2\int_0^h\left(1-\frac{z'}{h}\right)e^{-jk_0z'}\cdot\frac{e^{-jk_0r_0}}{r_0}\,dz' \tag{7}$$

with

$$r_0=\sqrt{z'^2+a^2}. \tag{8}$$

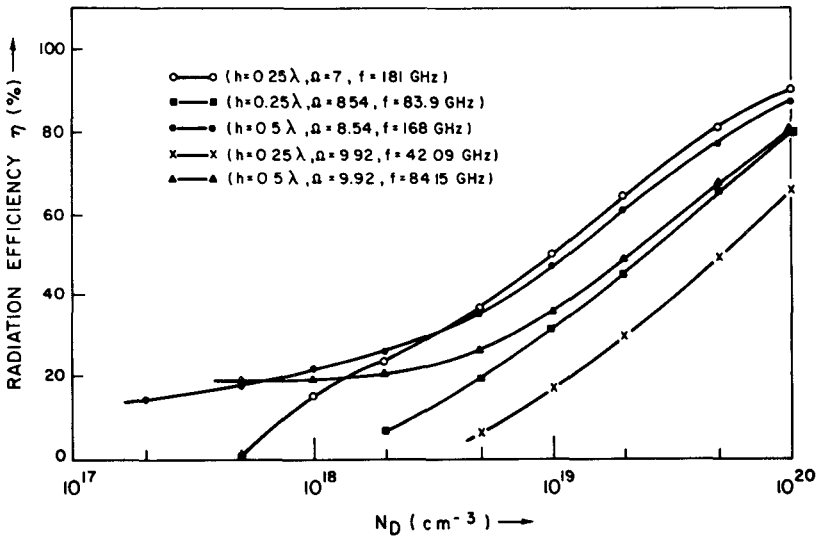

Fig. 2. Computed radiation efficiencies for tubular n-Si dipoles as a function of phosphorus doping concentration N_D.

Equation (1) yields the following approximate solution [7]:

$$I_z(Z) = \frac{2\pi V_0^e}{\zeta_0 \psi (1 - j/k_0 h)} \left[1 - \frac{|z|}{h}\right] e^{-jk_0|z|}. \quad (9)$$

Equation (9) represents a wave of current which travels outward from the generator at $z = 0$ towards both ends without reflection.

III. Numerical Computations

Numerical calculations based on the preceding theoretical development are presented to evaluate the performance of semiconductor dipole antennas operating in the frequency range of 42–362 GHz. For all the antennas that were analyzed, the internal impedance per unit length is well approximated by one of the following expressions:

$$Z^i(z) = r^i(z) + jx^i(z) = \frac{1}{2\pi a \sigma(z) d_s(z)} (1 + j) \quad (10)$$

or

$$Z^i(z) \cong r^i(z) = \frac{1}{2\pi a \sigma(z) d}, \quad (\text{when } d \ll d_s) \quad (11)$$

where the skin depth

$$d_s = \sqrt{\frac{2}{\omega \mu_0 \sigma}}. \quad (12)$$

$\sigma(z)$ is the conductivity (mho/meter) of the semiconductor and is related to the carrier concentration, which is equal to the doping concentration $N_D(z)$ if all the donors are ionized [11].

Case I: Computations have been performed for two solid dipoles ($a = 25$ μm, $\Omega = 2\ln(2h/a) = 8.54$) fabricated from n-Si ($N_D \approx 8 \times 10^{19}$ cm^{-3}). The half-wave dipole at 83.9 GHz has a radiation efficiency $\eta = 89$ percent while the full-wave dipole at 168 GHz has $\eta = 93$ percent.

Characteristics of various tubular dipoles (n-silicon over an insulating core) are presented in graphical form in Figs. 2 and 3. Fig. 2 is a plot of the radiation efficiency as a function of N_D in the semiconductor, while Fig. 3 displays the real and imaginary parts of the input admittance versus N_D. All these tubular dipoles have an outer radius $a = 25$ μm and a semiconductor coating of thickness $d = 2$ μm. It is clear from these figures that, for medium to high doping levels, semiconductor dipoles are efficient radiators at millimeter wavelengths and their input admittances fall in a practical range. In addition, our sample calculation for a $\lambda/2$ dipole ($\Omega = 7$, $N_D \simeq 4 \times 10^{19}$ cm^{-3}, $a = 25$ μm, $d = 2$ μm) at 362 GHz revealed a radiation efficiency $\eta = 86$ percent, indicating the viability of the proposed antennas in the submillimeter-wave regime as well.

Case II: Fig. 4 shows profiles of doping concentrations along several tubular dipoles ($a = 25$ μm, $d = 2$ μm) that yield pure traveling-wave distributions. The half-lengths of these antennas range from $k_0 h = \pi/2$ to $k_0 h = 4\pi$. The required values of N_D are all found to lie in a physically useful range of 10^{17} to 10^{20} cm^{-3}. Lower values of N_D are expected for n-GaAs and other high electron mobility semiconductor layers [11].

IV. Antenna Layout

The schematic of a monolithic semiconductor dipole antenna compatible with integrated circuit technology is shown in Fig. 5. The antenna structure consists of a semiconductor layer having an appropriate doping concentration profile. The semiconductor layer may be n-Si, n-GaAs, or another semiconductor material depending on its compatibility with the substrate. In the case of Si, it can be grown epitaxially on a high-resistivity Si substrate or on an insulating dielectric substrate such as sapphire.

The width w and the thickness t of the semiconductor layer are computed using the equivalent radii technique [8], [9]. For example, a tubular dipole having $h = 0.5\lambda$, $a = 25$ μm, $\Omega = 8.54$, $f = 168$ GHz, and $d = 2$ μm can be approximated by a semiconductor slab of $h = 0.5\lambda$, width $w = 100$ μm, and thickness $t \cong 2.5$ μm.

Fig. 5 also exhibits the use of surface field-effect in controlling the carrier concentrations along the antenna length. This is achieved by using a thin ($\simeq 1000$ °A) SiO_2 and/or Si_3N_4 layer and poly-Si gate electrodes grown on the Si layer to realize a metal–oxide–semiconductor (MOS)-type structure. The dc bias applied to the Si gates can be varied to deplete or accumulate carriers in the Si layer underneath the gate electrodes. The resistivity of the poly-Si electrodes is chosen to be sufficiently high so that they can modulate the conductivity $\sigma(z)$ of the

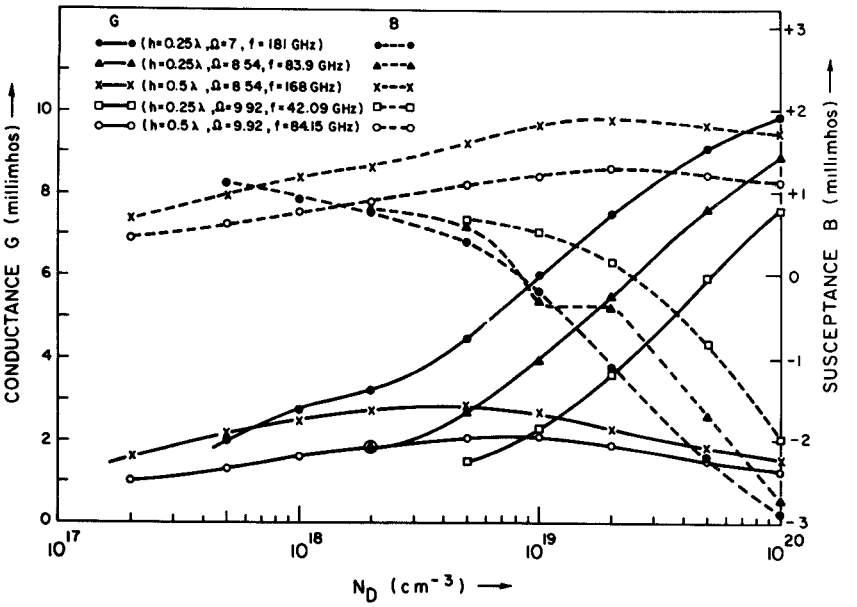

Fig. 3. Computed input admittances of tubular n-Si dipoles as a function of phosphorus doping concentration N_D.

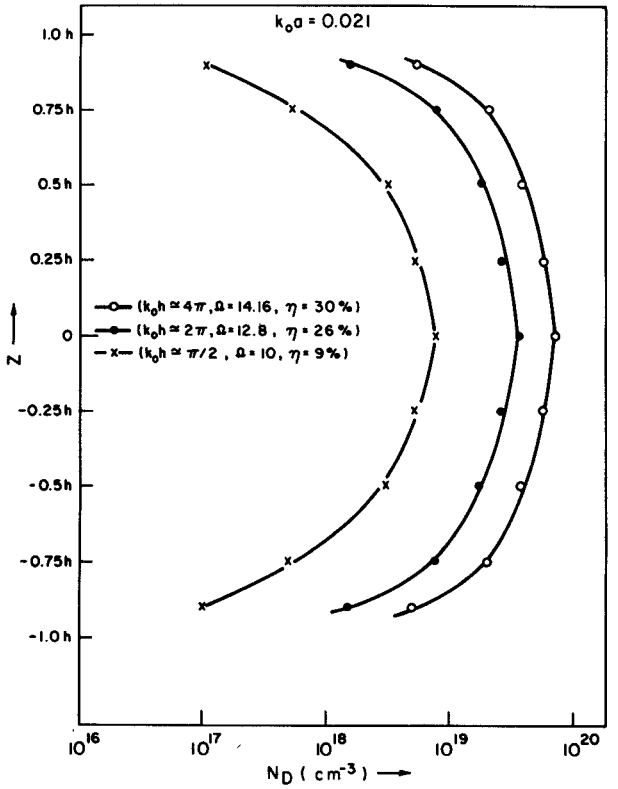

Fig. 4. Doping profiles of tubular traveling-wave antennas having tapered internal impedance per unit length $Z'(z)$.

antenna without interfering with its ac operation. (The use of high-resistivity lines in microwave receiver circuits has been discussed by Bassen [12]). Variations in $\sigma(z)$ change the antenna impedance per unit length $Z_i(z)$, and this in turn results in a modified current distribution $I_z(z)$ and radiation pattern. Alternate methods for manipulating carrier concentration may include biased p–n junctions, and optoelectronic means utilizing photoeffects to generate carriers along the antenna length in a predetermined way to realize a desired conductivity profile.

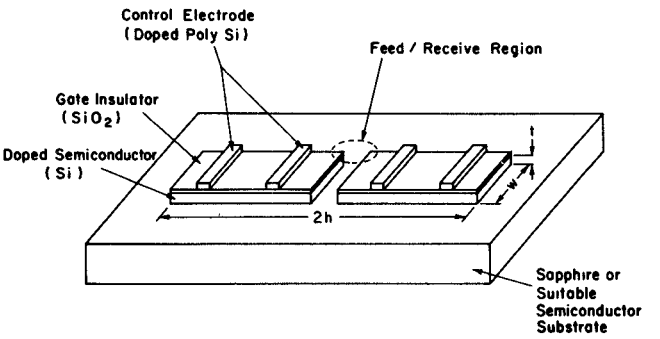

Fig. 5. A monolithic semiconductor dipole antenna structure with poly-Si control gates.

V. Conclusions

In summary, theoretical calculations have been presented to show that efficient semiconductor antennas can be realized at millimeter and submillimeter wavelengths. A practical design to implement these antennas in a monolithic configuration has also been discussed in the context of the present IC technology. Eventual integration of control circuitry and antenna arrays into a compact and agile system is foreseen.

References

[1] A. Chu, W. E. Courtney, and L. J Mahoney, "Monolithic circuits for millimeter-wave systems," *Microwave J.*, vol. 26, pp. 28–48, Feb 1983.

[2] F. C Jain, C. V. Valerio, and R. Bansal, "Conductivity modulated semiconductor antennas," *Bull. Am. Phys. Soc.*, vol. 28, p. 48, 1983.

[3] K. L. Klohn, R. E. Horn, H. Jacobs, and E. Freibergs, "Silicon waveguide frequency scanning linear array antenna," *IEEE Trans. Microwave Theory Tech.*, vol. MTT-26, pp. 764–773, Oct. 1978.

[4] K. R. Carver and J. W. Mink, "Microstrip antenna technology," *IEEE Trans. Antennas Propagat.*, vol. AP-29, pp. 2–24, Jan. 1981.

[5] R. W. P. King and T. T Wu, "The imperfectly conducting cylindrical transmitting antenna," *IEEE Trans. Antennas Propagat*, vol AP-14, pp. 524–534, Sept. 1966

[6] R. W. P. King, C W. Harrison, and E A. Aronson, "The imperfectly conducting cylindrical transmitting antenna: Numerical results," *IEEE Trans. Antennas Propagat.*, vol. AP-14, pp. 535–542, Sept. 1966.

[7] T. T. Wu and R. W P King, "The cylindrical antenna with nonreflecting resistive loading," *IEEE Trans Antennas Propagat.*, vol. AP-13, pp. 369–373, May 1965.

[8] C. A. Balanis, *Antenna Theory: Analysis and Design*. New York: Harper and Row, 1978.

[9] C. M. Butler, "The equivalent radius of a narrow conducting strip," *IEEE Trans Antennas Propagat*, vol. AP-30, pp. 755–758, July 1982.
[10] I. E. Rana and N. G Alexopoulos, "Current distribution and input impedance of dipoles," *IEEE Trans. Antennas Propagat.*, vol. AP-29, pp. 99–105, Jan. 1981.
[11] S. M. Sze, *Physics of Semiconductor Devices*, 2nd edition. New York: Wiley, 1981.
[12] H. Bassen, "RF/Microwave radiation measurement, risk assessment and control activities at the Bureau of Radiological Health," *IEEE Antennas Propagat Soc. Newsletter*, vol. 23, pp. 5–8, Apr. 1981

Dynamic Behavior of Pulsed-IMPATT Oscillators

R K. MAINS, G. I. HADDAD, D. BOWLING, AND M. AFENDYKIW

***Abstract*—A method of simulating the dynamic behavior of pulsed-IMPATT oscillators is presented. It is assumed that the simulation variables change slowly with respect to the RF period so that the quasi-static approximation may be used. A comparison of simulation results with experimental results for an *X*-band circuit is given.**

I. Introduction

The quasi-static approximation may be effectively used to simulate transient effects in free-running and injection-locked pulsed oscillators [1], [2]. It is an alternative to the time-consuming method of performing a complete device-circuit interaction simulation in the time domain using a small time step due to stability restrictions on the device simulation. The quasi-static method requires a complete steady-state characterization of the IMPATT device over the ranges of temperature, bias current density, and RF voltage amplitude that will be encountered in the transient simulation. It is then assumed that the simulation parameters change slowly with respect to the RF period so that the IMPATT appears to be in a steady-state condition at any particular instant of time. In this manner, the transient can readily be simulated over the entire pulse width.

II. IMPATT Device Model

Fig. 1 shows the doping profile of the GaAs double-drift IMPATT diode used in the simulations. This particular structure was fabricated by Microwave Associates, Inc., and was also used in the experimental phase of the investigation. This diode was simulated at 10 GHz using the computer programs developed by Bauhahn and Haddad [3], [4] and later modified by Mains and Haddad [5], wherein it is assumed that the particle currents consist of a drift plus diffusion term, with drift velocities and diffusion coefficients expressed as functions of the local electric field. Simulations were carried out at temperatures $T = 300$, 400, 500, 535, and 575° K. At each temperature, simulations were performed at bias current densities of $J_{dc} = 400$, 650, and 1000 A/cm^2. For each (T, J_{dc}) combination, a sinusoidal RF voltage at 10 GHz was applied and the amplitude was varied from zero to the point where the diode efficiency dropped significantly. The information thus obtained is Y_D $(f = 10$ GHz; $T, J_{dc}, V_{RF})$, the diode admittance in mho/cm^2, and V_{dc} $(f = 10$ GHz; $T, J_{dc}, V_{RF})$, the diode large-signal operating voltage. At $J_{dc} = 0$, the diode is modeled as a depletion capacitance $C_0 = (\epsilon A / w_d)F$ in series with a small resistor $R_0 = (w_u/\sigma A)\Omega$ to account for the undepleted region (w_d is the depletion region width and w_u is the width of the undepleted region). To obtain the diode characteristics at operating points other than those simulated, a linear interpolation scheme is used [2].

It is assumed that the circuit admittance $Y_c(s)$ varies more rapidly with frequency than the diode admittance so that Y_D may be assumed constant with frequency over the range of interest. However, the diode cold capacitance $C_D = (\epsilon / w)$ F/cm^2 (where $w = w_d + w_u = 6.95$ μm) is lumped into $Y_c(s)$ so that the ωC_D component of the diode susceptance does vary with frequency. The device area was assumed to be $A = 1.3 \times 10^{-3}$ cm^2, which is the measured value for the diode.

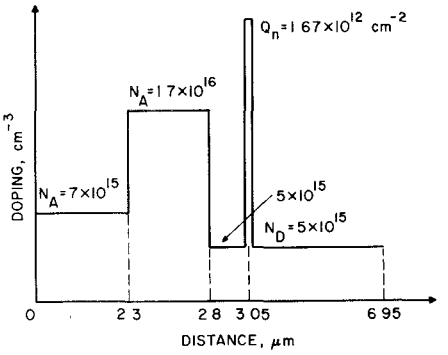

Fig. 1. Doping profile of GaAs IMPATT diode used in the theoretical and experimental investigations (diode area $A = 1.3 \times 10^{-3}$ cm^2).

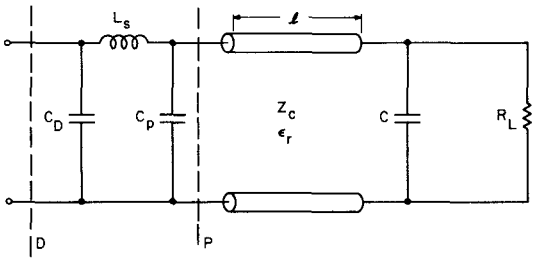

Fig. 2. Circuit model used for the simulations ($C_D = 2.07$ pF, $L_s = 0.153$ nH, $C_p = 0.32$ pF, $Z_c = 3.98$ Ω, $\epsilon_r = 2.53$, $l = 0.2667$ cm, $C = 0.111$ pF, and $R_L = 50$ Ω).

III. Circuit Model

Fig. 2 shows the circuit used to model the actual oscillator circuit, which consists of a 50-Ω transmission line (represented by R_L) and a low-impedance transformer adjacent to the diode package (represented by Z_c, l, and ϵ_r). The capacitance C is the discontinuity capacitance between the 50-Ω transmission line and the transformer. The circuit elements to the right of plane P were verified from experimental impedance measurements at this plane. It was attempted to measure the package-mounting equivalent circuit elements L_s and C_p; however some uncertainty remained concerning these values, especially for the series inductance L_s. The procedure was to use the experimentally determined value of 0.32 pF for C_p and to determine L_s as follows. The diode admittance resulting from the simulation at $T = 500$°K, $J_{dc} = 650$ A/cm^2 (the bias current density used experimentally) and $V_{RF} =$

Manuscript received June 29, 1983; revised October 7, 1983. This work was supported in part by the Naval Weapons Center, China Lake, CA

R. K. Mains and G. I. Haddad are with the Electron Physics Laboratory, Department of Electrical and Computer Engineering, University of Michigan, Ann Arbor

D. Bowling and M. Afendykiw are with the Naval Weapons Center, China Lake, CA 93555.

0018-9480/84/0200-0208$01.00 ©1984 IEEE